Applied Physics Letters

Tunable underwater acoustic metamaterials via quasi-Helmholtz resonance: From low-frequency to ultra-broadband

Cite as: Appl. Phys. Lett. **118**, 071904 (2021); https://doi.org/10.1063/5.0028135
Submitted: 05 September 2020 . Accepted: 05 February 2021 . Published Online: 18 February 2021

Mingyu Duan, Chenlei Yu, Fengxian Xin, and Tian Jian Lu

View Online Export Citation CrossMark

ARTICLES YOU MAY BE INTERESTED IN

Broadband sound attenuation by metaliner under grazing flow
Applied Physics Letters **118**, 063504 (2021); https://doi.org/10.1063/5.0042228

Acoustic impedance regulation of Helmholtz resonators for perfect sound absorption via roughened embedded necks
Applied Physics Letters **117**, 151904 (2020); https://doi.org/10.1063/5.0024804

Manually tunable ventilated metamaterial absorbers
Applied Physics Letters **118**, 053504 (2021); https://doi.org/10.1063/5.0037547

Challenge us.
What are your needs for periodic signal detection?
Watch

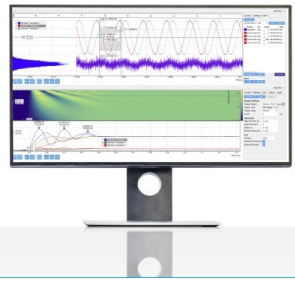

Zurich Instruments

AIP Publishing

© 2021 Author(s).

Applied Physics Letters ARTICLE scitation.org/journal/apl

Tunable underwater acoustic metamaterials via quasi-Helmholtz resonance: From low-frequency to ultra-broadband

Cite as: Appl. Phys. Lett. **118**, 071904 (2021); doi: 10.1063/5.0028135
Submitted: 5 September 2020 · Accepted: 5 February 2021 ·
Published Online: 18 February 2021

View Online Export Citation CrossMark

Mingyu Duan,[1,2] Chenlei Yu,[1,2] Fengxian Xin,[1,2,a)] and Tian Jian Lu[3,4,b)]

AFFILIATIONS

[1]State Key Laboratory for Strength and Vibration of Mechanical Structures, Xi'an Jiaotong University, Xi'an 710049, People's Republic of China
[2]MOE Key Laboratory for Multifunctional Materials and Structures, Xi'an Jiaotong University, Xi'an 710049, People's Republic of China
[3]State Key Laboratory of Mechanics and Control of Mechanical Structures, Nanjing University of Aeronautics and Astronautics, Nanjing 210016, People's Republic of China
[4]MIIT Key Laboratory of Multi-Functional Lightweight Materials and Structures, Nanjing University of Aeronautics and Astronautics, Nanjing 210016, People's Republic of China

[a)]**Author to whom correspondence should be addressed:** fengxian.xin@gmail.com
[b)]**Electronic mail:** tjlu@nuaa.edu.cn

ABSTRACT

We report a lightweight tunable acoustic metamaterial with deep subwavelength thickness (e.g., $\lambda/300$) and strong load-bearing capability for underwater low-frequency and ultra-broadband acoustic perfect absorption. The metamaterial is constructed by introducing a rubber coating and an embedded metallic neck into a metallic hexagonal honeycomb Helmholtz resonator. Physically, the quasi-Helmholtz resonance triggered by the rubber coating together with the anti-phase cancellation caused by the embedded neck leads to superior sound absorption. Theoretical predictions of the metamaterial performance agree well with finite element simulation results. With fixed external morphology (e.g., honeycomb-cored sandwich panel) and fixed overall thickness (e.g., 50 mm), key internal geometrical parameters of the proposed metamaterial can be tailored to achieve tunable perfect absorption from, e.g., 100 Hz to 300 Hz. Further, combining such tunable quasi-Helmholtz resonance leads to ultra-broadband quasi-perfect absorption from, e.g., 306 Hz to 921 Hz. This work contributes to designing underwater acoustic metamaterials and controlling underwater acoustic waves.

Published under license by AIP Publishing. https://doi.org/10.1063/5.0028135

Underwater acoustic invisibility, underwater acoustic communications, and underwater acoustic device design are all dependent upon acoustic wave absorption and control. Because of the long wavelength of a low-frequency acoustic wave, it is difficult for the classical underwater acoustic absorbers[1–7] with rigid backing and deep subwavelength thickness to achieve perfect and broadband underwater sound absorption below 1000 Hz. Recent emergence of acoustic metamaterials provides a possibility to address this critical issue.[8–16] In airborne acoustics, acoustic metamaterials built upon Helmholtz resonance[17–25] and Fabry–Pérot resonance[26–32] have been successfully developed to realize low-frequency perfect absorption across deep subwavelength scale. Nonetheless, due to the high bulk modulus and low viscosity of water, both the Helmholtz resonance and the Fabry–Pérot resonance are unable to achieve efficient underwater sound absorption at low frequencies. Thus, at present, underwater sound absorption metamaterials are mainly based on local resonance, primarily for sound absorption up to the kilohertz level.[33–38] Development of acoustic metamaterials with underwater low-frequency broadband absorption performance remains elusive.

In this work, we present a type of quasi-Helmholtz resonance by introducing a rubber coating and an embedded neck into the classical Helmholtz resonance cavity, as shown in Fig. 1(b). Since the rubber coating provides sufficient elasticity and damping, it is possible to realize efficient low-frequency underwater sound absorption. On this basis, a deep subwavelength acoustic metamaterial is constructed, as shown in Fig. 1(a), and its underwater acoustic performance is

Published under license by AIP Publishing

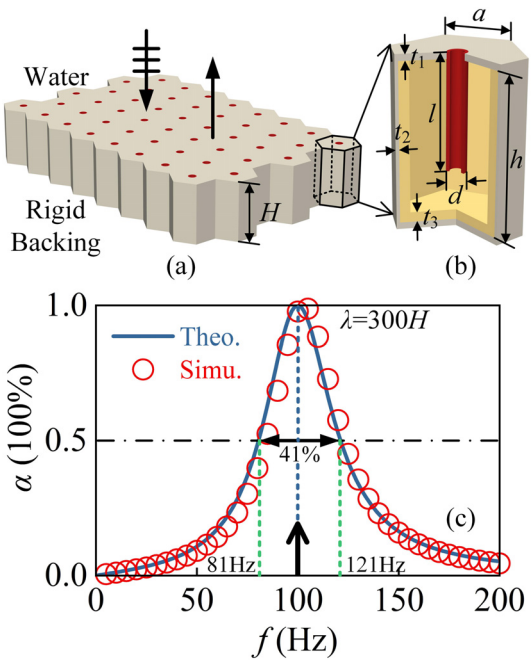

FIG. 1. (a) Geometry of the proposed metamaterial with thickness $H = 50$ mm. (b) Cutaway view of one representative unit with side length $a = 20$ mm, cavity height $h = 48$ mm, facesheet thickness $t_1 = 2$ mm, honeycomb wall thickness $2t_2 = 2$ mm, rubber coating thickness $t_3 = 9.23$ mm, embedded neck diameter $d = 2.09$ mm, and embedded neck length $l = 35.47$ mm. (It should be clarified that these parameters are only selected as an example to demonstrate the superior sound absorption performance of the metamaterial. Future work should be to study the sensitivity of absorption and resonance frequency to metamaterial design geometry.) (c) Sound absorption coefficient of the metamaterial. Blue curve and red circles represent theoretical predictions and finite element (FE) simulation results, respectively.

investigated by a combined analytical and numerical approach. It is demonstrated that the proposed metamaterial having deep subwavelength thickness exhibits tunable low-frequency acoustic perfect absorption. Upon parallel design of the metamaterial units, we further realize low-frequency broadband perfect absorption at the hundred hertz level by combined quasi-Helmholtz resonance.

The proposed metamaterial is constructed by introducing an embedded neck and a rubber coating into a Helmholtz resonator and then placing such resonators periodically in a honeycomb-cored sandwich panel, as shown in Figs. 1(a) and 1(b). Both the sandwich panel and the embedded neck are made of steel, which can be simplified to be acoustically rigid due to the excellent stiffness of the sandwich construction. The embedded neck is a hollow cylinder, which enables water flowing into/out of the resonator under acoustic excitation and hence provides acoustic mass and acoustic resistance for the resonator. The rubber coating with elasticity and damping is bonded to the inner sidewalls and the bottom surface of the resonator cavity to provide additional acoustic resistance and acoustic capacitance and trigger the quasi-Helmholtz resonance. The embedded neck and rubber coating also provides tunability to tailor the acoustic properties of the metamaterial. Through adjusting the geometries of the neck and rubber coating, acoustic impedance tuning can be realized while maintaining the external morphology and thickness of the metamaterial unchanged. The proposed metamaterial also exhibits multifunctional attributes: the metallic honeycomb sandwich panel can carry large structural load, while the quasi-Helmholtz resonators can realize underwater acoustic perfect absorption, and these are achieved at lightweight and deep subwavelength thickness of the sandwich panel.

According to previous works,[3,5,35,36,39–41] it is assumed that the backing condition of the metamaterial is rigid to simplify the analysis (the acoustic performance of the metamaterial with water/air backing is analyzed in the supplementary material). In such a case, the sound absorption coefficient of the metamaterial can be calculated by

$$\alpha = 1 - |R|^2 = 1 - |(Z_s - 1)/(Z_s + 1)|^2, \tag{1}$$

where R is the reflection coefficient and Z_s is the surface acoustic impedance ratio of the metamaterial. To determine Z_s, we need to calculate the acoustic impedance of the resonator cavity and the embedded neck. The resonator cavity consisted of rubber coating and water cavity. According to the electro-acoustic analogy method, the acoustic impedances of the rubber coating and the water cavity are in parallel connection (see the details in the supplementary material). Therefore, the total acoustic impedance of the resonator cavity can be expressed by

$$Z_c = \frac{1}{\frac{1}{Z_r} + \frac{1}{Z_w}}, \tag{2}$$

where Z_r and Z_w are the acoustic impedance of the rubber coating and water cavity, respectively. The acoustic impedance of the rubber coating is

$$Z_r = -jS_c\rho_r c_r^2/(\omega V_r), \tag{3}$$

where j is the imaginary unit, $V_r = S_c h - S_w(h - t_3)$ is the volume of the rubber coating, $S_c = 1.5\sqrt{3}(a - t_2/\sqrt{3})^2$ and $S_w = 1.5\sqrt{3}(a - t_2/\sqrt{3} - 2t_3/\sqrt{3})^2$ are separately the cross-sectional area of the resonator cavity and the water cavity, respectively, ρ_r and c_r are separately the density and longitudinal wave velocity of rubber, respectively, $\omega = 2\pi f$ is the angular frequency, and f is the frequency.

Linear viscoelastic constitutive laws are commonly employed to describe the elasticity and damping behaviors of rubber materials in underwater acoustic absorbers.[3–7,36–38] Specifically, the complex bulk modulus $\tilde{K}_r = (1 + j\eta_r)K_r$ is introduced to express the longitudinal acoustic wave velocity as $c_r = \sqrt{\tilde{K}_r/\rho_r}$, where $K_r = \frac{E_r(1-\nu_r)}{(1+\nu_r)(1-2\nu_r)}$, η_r, E_r, and ν_r are the bulk modulus, loss factor, Young's modulus, and Poisson ratio of rubber, respectively. Actually, the loss factor of rubber Young's modulus is usually frequency dependent. However, the target frequency range in this work is relatively narrow; thus, the loss factor is assumed to be frequency independent in reference to the previous works,[3–7,35–37,42] so as to simplify the calculation and analysis. As a future work, the frequency dependent Young's modulus can be considered to account for the viscoelastic dispersion in the rubber coating. Following Meng *et al.*'s work,[7] the density, loss factor, Young's modulus, and Poisson ratio of rubber are selected as $\rho_r = 1100\text{kg/m}^3$, $\eta_r = 0.3$, $E_r = 10$ MPa, and $\nu_r = 0.49$, respectively.

The acoustic impedance of the water cavity can be expressed by

$$Z_w = -jS_c\rho_0 c_0^2/(\omega V_w), \tag{4}$$

Published under license by AIP Publishing

where $\rho_0 = 1000\text{kg/m}^3$ and $c_0 = 1500\text{m/s}$ are the density and acoustic wave velocity of water, respectively, $V_w = S_w(h - t_3) - S_n(l - t_1)$ is the volume of the water cavity excluding the embedded neck, and $S_n = \pi d^2/4$ is the inner cross-sectional area of the embedded neck. Finally, the total acoustic impedance of the resonator can be obtained by substituting Eqs. (3) and (4) into Eq. (2).

The acoustic impedance of the embedded neck is given by[43]

$$Z_n = \frac{j\omega\rho_0 l}{\varphi}\left[1 - \frac{2J_1\left(y\sqrt{-j}\right)}{\left(y\sqrt{-j}\right)J_0\left(y\sqrt{-j}\right)}\right]^{-1} + \frac{\sqrt{2}\eta_0 y}{\varphi d} + j\frac{0.85\omega\rho_0 d}{\varphi}, \tag{5}$$

where $\varphi = S_n/S_c$ is the perforation ratio of the facesheet, $J_n(X)$ is the nth-order first class Bessel function, $y = (d/2)/\sqrt{\eta_0/\rho_0\omega}$ is the ratio of the embedded neck radius to the viscous boundary layer thickness, and $\eta_0 = 1.01 \times 10^{-3}\,\text{Pa}\cdot\text{s}$ is the dynamic viscosity of water. By adjusting the dimensions of the rubber coating and the embedded neck, the acoustic impedance of the metamaterial can be tuned under constant external morphology. Finally, the surface acoustic impedance ratio of the metamaterial is expressed by

$$Z_s = \delta Z = \delta(Z_n + Z_c)/Z_0, \tag{6}$$

where $Z = (Z_n + Z_c)/Z_0$ is the surface acoustic impedance ratio of the resonator, and $\delta = 1.5\sqrt{3}a^2/S_c$ is the area correction factor applied to describe the influence of honeycomb wall thickness on the acoustic impedance. By substituting (5) into (1), the sound absorption coefficient of the metamaterial can be theoretically predicted.

To validate the above theoretical predictions, finite element (FE) simulations are performed with COMSOL[44] (see the supplementary material for modeling details). To verify the reliability of the rigid assumption in the theoretical model, a complete FE model considering the acoustic-structure coupling between water and steel honeycomb is established in the supplementary material. The results show that the influence of acoustic-structure coupling between water and steel on the metamaterial performance is negligible due to the mechanical strengthening of the honeycomb walls (see the supplementary material for details), so the rigid assumption in the theoretical model and FE model is accurate and reliable. Therefore, to simplify the calculation and analysis, the rigid assumption is also adopted in the following FE models. As shown in Fig. 1(c), theoretical predictions agree well with FE simulation results. The proposed metamaterial achieves acoustic perfect absorption ($\alpha > 99\%$) at 100 Hz, with a semi-absorption bandwidth of 41%. At the absorption peak, the acoustic wavelength λ is 300 times the metamaterial thickness H, implying that perfect absorption is realized at the deep subwavelength scale.

To understand the physical mechanisms underlying the superior sound absorption performance of the proposed metamaterial, acoustic pressure distribution in water is plotted in Fig. 2(a). An acoustic pressure drop occurs in the embedded neck, causing a phase difference. While, in the water cavity, the acoustic pressure distributes equally because of the long wavelength of the low-frequency acoustic wave. The phase difference $\Delta\phi$ between the metamaterial surface and the rubber coating surface is calculated and plotted in Fig. 2(b). The value of $\Delta\phi$ is $\pi/2$ at about 100 Hz. Correspondingly, phase difference between the incident acoustic wave and the reflected acoustic wave is equal to π, resulting in anti-phase cancellation at the metamaterial surface. It should be noticed that the elasticity of rubber coating also plays

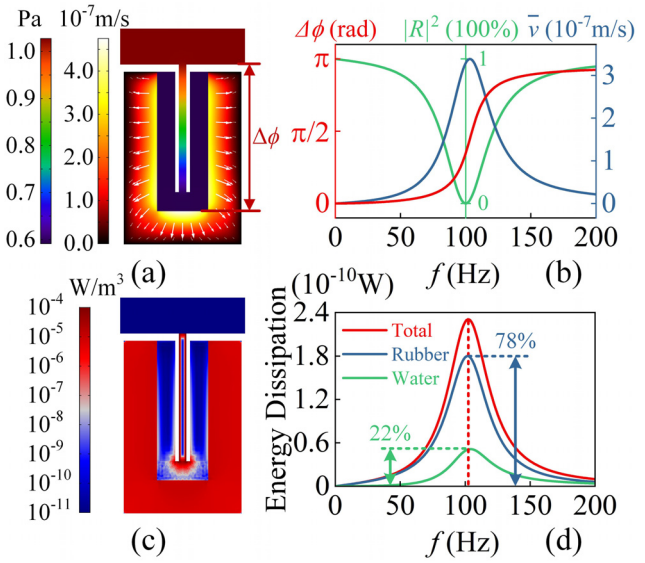

FIG. 2. (a) Sectional view of the acoustic pressure distribution and particle velocity distribution at the absorption peak frequency, with white arrows indicating velocity direction in rubber coating. (b) Reflection coefficient (green curve), phase difference between surfaces of the metamaterial and rubber coating (red curve), and the average particle velocity of the rubber coating surface (blue curve). (c) Sectional view of energy dissipation density in the metamaterial at absorption peak frequency. (d) Energy dissipation in different pathways in the metamaterial.

an important role in the phase modulation of acoustic wave. In the absence of the rubber coating, it is impossible to achieve $\Delta\phi = \pi/2$ at such a low-frequency due to the high bulk modulus of water. Because the incident acoustic energy is trapped and dissipated in the resonator cavity, the reflection coefficient shown in Fig. 2(b) is equal to 0 at 100 Hz. The acoustic wave in the resonator triggers acoustic-structure coupling vibration between water and rubber shown in Fig. 2(a), causing the rubber coating surface to experience a compressive vibration. Figure 2(b) shows that the average velocity of the rubber coating surface is maximized around the absorption peak frequency.

Figure 2(c) presents the energy dissipation density in the metamaterial. It is seen that energy dissipation mainly occurs inside and at the end of the embedded neck and in the rubber coating. The former two are similar to those in the classical Helmholtz resonance, while the latter one is a type of energy dissipation triggered by rubber coating. To clarify the proportion of each type of energy dissipation, the total energy dissipation density, the energy dissipation density in rubber, and the energy dissipation density in water are separately calculated and plotted in Fig. 2(d). The total energy dissipation, the energy dissipation in rubber, and that in water are all maximized at about 100 Hz, i.e., the absorption peak frequency. Additionally, the energy dissipated in rubber accounts for 78% of the total energy dissipation, while in water it accounts for only 22%. Energy dissipation in rubber is therefore dominant, which is fundamentally different from the dissipation mechanism of the classical Helmholtz resonance. Compared with Helmholtz resonance in air, water by itself cannot provide enough acoustic capacitance and acoustic resistance for sound absorption, thus limiting the application of classical Helmholtz resonance in water.

Published under license by AIP Publishing

However, the proposed metamaterial squarely addresses this deficiency by constructing an acoustic-structure coupling resonant system. A quasi-Helmholtz resonance dominated by rubber coating is demonstrated, which leads to superior sound absorption performance of the proposed metamaterial.

In practical applications, acoustic metamaterials are often required to exhibit tunable and broadband acoustic performance. Upon adjusting the rubber coating thickness t_3, the embedded neck length l, and the embedded neck diameter d, the tunable absorption performance of the present metamaterial can be achieved, as shown in Fig. 3(a). It is seen that Samples A–C of the metamaterial realize perfect absorption at 100, 200, and 300 Hz, respectively. The thickness of these samples is fixed at 50 mm, corresponding to $\lambda/300$, $\lambda/200$, and $\lambda/100$ (see the supplementary material for detailed geometric parameters of the samples). Such tunable performance is attributed to the acoustic impedance regulation by the rubber coating and the embedded neck. Equation (1) dictates that, to achieve perfect absorption ($\alpha = 1$), acoustic reactance $\mathrm{Im}(Z_s) = 0$ and acoustic resistance $\mathrm{Re}(Z_s) = 1$ need to hold simultaneously. However, because the acoustic resistance and acoustic reactance of the metamaterial do not exist independently, the above impedance matching condition cannot be strictly satisfied. Generally, perfect absorption appears when $\mathrm{Im}(Z_s)$ is equal to 0 and $\mathrm{Re}(Z_s)$ is around 1. As shown in Figs. 3(b)–3(d), the difference in internal geometry enables the samples to acquire different acoustic impedances. As a result, $\mathrm{Im}(Z_s)$ of the samples is dropped to 0 and the $\mathrm{Re}(Z_s)$ is approximately equal to 1 at 100, 200, and 300 Hz, respectively, resulting in the tunable perfect absorption peak.

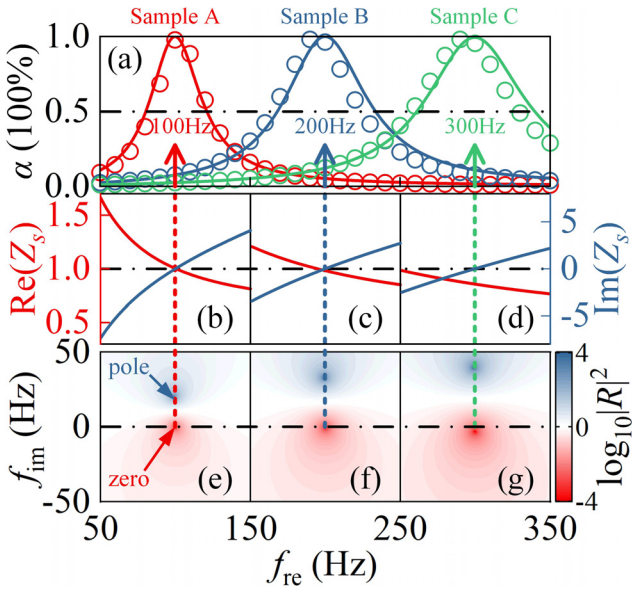

FIG. 3. (a) Tunable sound absorption coefficient of Samples A–C. Colored curves and circles represent theoretical predictions and FE simulation results, respectively. Colored arrows indicate the absorption peak frequency. (b)–(d) Corresponding acoustic resistance (red curves) and acoustic reactance (blue curves) of the samples. (e)–(g) Complex frequency plane description of the corresponding reflection coefficient of the samples. All figures share the same *x*-axis with (e)–(g).

We further discuss the acoustic performance of each sample via complex frequency plane analysis,[45] as shown in Figs. 3(e)–3(g). Complex frequency plane analysis is a method developed in recent years to analyze the sound absorption performance of various acoustic absorbers.[17,18,28,29,31,46] Through complex frequency plane analysis, the perfect absorption performance and damping state of the sound absorbers can be clearly analyzed.[31,47] If the frequency is extended to the complex number domain as $f = f_{re} + jf_{im}$, the reflection coefficient of the resonator can be expressed as a function of f_{re} and f_{im} and plotted in complex frequency plane. For the lossless case, the reflection coefficient has a pair of zero and pole points that are conjugate symmetric about the real frequency axis (i.e., $f_{im} = 0$), where the complex number is related to the energy leakage of the radiation.[45] The zero and pole point are the minimum value (i.e., $R = 0$) and maximum value of the reflection coefficient, respectively. In a realistic lossy system, the introduction of damping will cause the zero point and pole point shift up together with the shape change of the zero-pole pair. When the zero point just falls on the real frequency axis, the energy leakage of the system can be completely balanced by the loss, so that the perfect absorption can be achieved. Figures 3(e)–3(g) demonstrate that the zero points of the three samples fall on the real frequency axis at 100, 200, and 300 Hz, respectively, consistent with the perfect absorption peaks of Fig. 3(a). Besides, the distance between the zero point and the pole point increases with increasing perfect absorption frequency, thus broadening the acoustic semi-absorption bandwidth, as shown in Fig. 3(a).

Based on the acoustic impedance tunability of the present metamaterial, a wide absorption band can be constructed by paralleling multiple metamaterial units with tailored acoustic impedances. For illustration, we construct a 16-unit parallel sample as shown in Fig. 4(a) and set it as the smallest periodic unit of the metamaterial. The surface acoustic impedance ratio of the parallel sample can be expressed as $Z_s = 16\delta \cdot \left(\sum_{k=1}^{K=16} \frac{1}{Z_k} \right)^{-1}$, where Z_k is the surface acoustic impedance ratio of the kth resonator. As shown in Fig. 4(a), upon tailoring the internal geometric parameters of each unit (see the supplementary material for details), the parallel sample achieves ultra-broadband acoustic quasi-perfect absorption ($\alpha > 0.9$) from 306 Hz to 921 Hz with a deep subwavelength thickness of 50 mm. The theoretical predictions agree well with FE simulation results. It should be noticed that each unit cell in the parallel sample is an imperfect acoustic absorber with a single absorption peak value lower than 0.9, but the parallel sample composed of these unit cells exhibits extraordinary broadband quasi-perfect sound absorption performance. This is due to the combination effect of the quasi-Helmholtz resonance, the direct parallel summation of 1/Z results in flat impedance, namely, the acoustic resistance and acoustic reactance of the sample are separately around 1 and 0 from 306 Hz to 921 Hz, as shown in Fig. 4(b). We further analyze the reflection coefficient of the parallel sample in complex frequency plane, as shown in Fig. 4(c). It is seen that the multiple zero points are combined together to construct the acoustic quasi-perfect absorption band, as shown by the contour line of $\alpha = 0.9$. Because all the zero points lie above the real frequency axis, each unit of the sample is an imperfect absorber in an overdamped state. Thus, in contrast with achieving broadband absorption by simply combining perfect absorbers, the sound absorption coefficient curve of the 16-unit

Published under license by AIP Publishing

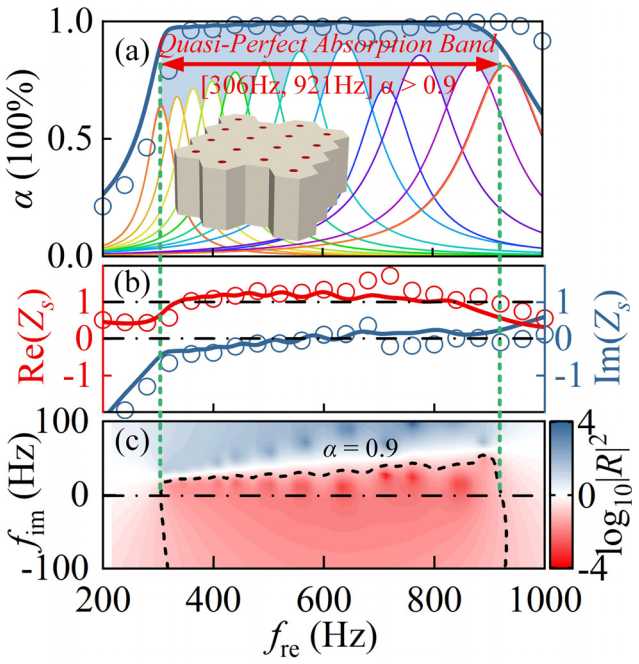

FIG. 4. (a) Ultra-broadband acoustic quasi-perfect absorption of the 16-unit parallel sample. Blue curves and circles are the sound absorption coefficient of the parallel sample. Rainbow colored curves are the sound absorption coefficient of the 16 units, and some of them are coincident. (b) Acoustic resistance (red) and acoustic reactance (blue) of the 16-unit parallel sample. Curves and circles represent theoretical predictions and FE simulation results, respectively. (c) Complex frequency plane description of the reflection coefficient of the 16-unit parallel sample. The dashed line marks the contour of $|R|^2 = 0.1$, i.e., $\alpha = 0.9$. All figures share the same *x*-axis with (c).

parallel sample without significant absorption valleys is smoother. Consequently, the overall sound absorption performance of the proposed metamaterial is superior.

In this Letter, we propose a deep subwavelength acoustic metamaterial for acoustic perfect absorption. Mechanism analysis shows that a kind of quasi-Helmholtz resonance is triggered by rubber coating in the metamaterial, causing the low-frequency acoustic perfect absorption. Upon tailoring the internal geometric parameters of the proposed metamaterial, tunable low-frequency and ultra-broadband perfect absorption are achieved while maintaining its external morphology and fixing its thickness at the deep subwavelength scale. This work has important implications for underwater acoustic metamaterial design and underwater acoustic wave control.

See the supplementary material for the details of the acoustic impedance of the resonator cavity, the finite element model, the rigidity simplification validation of the steel parts, and the geometric parameters of samples, as well as the influence of the backing on the acoustic performance of the metamaterial.

This work was supported by the National Natural Science Foundation of China (Nos. 52075416, 11772248, 11761131003, and U1737107) and the Open Fund of the State Key Laboratory of Mechanics and Control of Mechanical Structures (Nos. MCMS-I-0219K01 and MCMS-E-0219K02).

DATA AVAILABILITY

The data that support the findings of this study are available from the corresponding author upon reasonable request.

REFERENCES

[1]R. Lane, Ultrasonics **19**, 28 (1981).
[2]S. M. Ivansson, J. Acoust. Soc. Am. **119**, 3558 (2006).
[3]C. Ye, X. Liu, F. Xin, and T. J. Lu, J. Sound Vib. **426**, 54 (2018).
[4]D. Zhao, H. Zhao, H. Yang, and J. Wen, Appl. Acoust. **140**, 183 (2018).
[5]Z. Wang, Y. Huang, X. Zhang, L. Li, M. Chen, and D. Fang, J. Sound Vib. **479**, 115375 (2020).
[6]J. Wen, H. Zhao, L. Lv, B. Yuan, G. Wang, and X. Wen, J. Acoust. Soc. Am. **130**, 1201 (2011).
[7]H. Meng, J. Wen, H. Zhao, and X. Wen, J. Sound Vib. **331**, 4406 (2012).
[8]Z. Liu, X. Zhang, Y. Mao, Y. Y. Zhu, Z. Yang, C. T. Chan, and P. Sheng, Science **289**, 1734 (2000).
[9]P. Sheng, X. X. Zhang, Z. Liu, and C. T. Chan, Physica B **338**, 201 (2003).
[10]N. Fang, D. Xi, J. Xu, M. Ambati, W. Srituravanich, C. Sun, and X. Zhang, Nat. Mater. **5**, 452 (2006).
[11]Z. Yang, J. Mei, M. Yang, N. H. Chan, and P. Sheng, Phys. Rev. Lett. **101**, 204301 (2008).
[12]J. Mei, G. Ma, M. Yang, Z. Yang, W. Wen, and P. Sheng, Nat. Commun. **3**, 756 (2012).
[13]G. Ma and P. Sheng, Sci. Adv. **2**, e1501595 (2016).
[14]M. Yang and P. Sheng, Annu. Rev. Mater. Res. **47**, 83 (2017).
[15]A. J. Hicks, M. R. Haberman, and P. S. Wilson, J. Acoust. Soc. Am. **138**, EL254 (2015).
[16]V. Leroy, A. Strybulevych, M. Lanoy, F. Lemoult, A. Tourin, and J. H. Page, Phys. Rev. B **91**, 020301 (2015).
[17]N. Jiménez, W. Huang, V. Romero-García, V. Pagneux, and J. P. Groby, Appl. Phys. Lett. **109**, 121902 (2016).
[18]N. Jiménez, V. Romero-García, V. Pagneux, and J.-P. Groby, Sci. Rep. **7**, 13595 (2017).
[19]H. Long, Y. Cheng, and X. Liu, Appl. Phys. Lett. **111**, 143502 (2017).
[20]Y. Tang, S. Ren, H. Meng, F. Xin, L. Huang, T. Chen, C. Zhang, and T. J. Lu, Sci. Rep. **7**, 43340 (2017).
[21]Y. Tang, F. Xin, L. Huang, and T. Lu, Europhys. Lett. **118**, 44002 (2017).
[22]L.-J. Li, B. Zheng, L.-M. Zhong, J. Yang, B. Liang, and J.-C. Cheng, Appl. Phys. Lett. **113**, 103501 (2018).
[23]X. Wu, K. Y. Au-Yeung, X. Li, R. C. Roberts, J. Tian, C. Hu, Y. Huang, S. Wang, Z. Yang, and W. Wen, Appl. Phys. Lett. **112**, 103505 (2018).
[24]S. Huang, X. Fang, X. Wang, B. Assouar, Q. Cheng, and Y. Li, J. Acoust. Soc. Am. **145**, 254 (2019).
[25]J. Carbajo, S. G. Mosanenzadeh, S. Kim, and N. X. Fang, Appl. Phys. Lett. **116**, 054101 (2020).
[26]C. Zhang and X. Hu, Phys. Rev. Appl. **6**, 064025 (2016).
[27]C. Chen, Z. Du, G. Hu, and J. Yang, Appl. Phys. Lett. **110**, 221903 (2017).
[28]Y. Wang, H. Zhao, H. Yang, J. Zhong, D. Zhao, Z. Lu, and J. Wen, J. Appl. Phys. **123**, 185109 (2018).
[29]Y. Shen, Y. Yang, X. Guo, Y. Shen, and D. Zhang, Appl. Phys. Lett. **114**, 083501 (2019).
[30]L. Liu, H. Chang, C. Zhang, and X. Hu, Appl. Acoust. **111**, 083503 (2017).
[31]H. Long, C. Shao, C. Liu, Y. Cheng, and X. Liu, Appl. Phys. Lett. **115**, 103503 (2019).
[32]S. Kumar and H. P. Lee, Appl. Phys. Lett. **116**, 134103 (2020).
[33]H. Jiang, Y. Wang, M. Zhang, Y. Hu, D. Lan, Y. Zhang, and B. Wei, Appl. Phys. Lett. **95**, 104101 (2009).
[34]H. Jiang and Y. Wang, J. Acoust. Soc. Am. **132**, 694 (2012).
[35]T. Lee and H. Iizuka, Appl. Phys. Lett. **113**, 101903 (2018).
[36]J. Mei, X. Zhang, and Y. Wu, J. Appl. Phys. **123**, 091710 (2018).
[37]K. Shi, G. Jin, R. Liu, T. Ye, and Y. Xue, Results Phys. **12**, 132 (2019).
[38]H. Yang, H. Zhao, J. Yin, and J. Wen, AIP Adv. **9**, 125226 (2019).
[39]C. Ye, X. Liu, F. Xin, and T. J. Lu, ASME J. Vib. Acoust. **141**, 041006 (2019).

Published under license by AIP Publishing

[40]N. Gao and K. Lu, Appl. Acoust. **169**, 107500 (2020).
[41]H. Zou, P. Li, and P. Peng, Phys. Lett. A **384**, 126151 (2020).
[42]J. Zhong, H. Zhao, H. Yang, J. Yin, and J. Wen, Appl. Acoust. **145**, 104 (2019).
[43]D. Y. Maa, J. Acoust. Soc. Am. **104**, 2861 (1998).
[44]See cn.comsol.com for COMSOL Multiphysics®, version 5.4, COMSOL AB, Stockholm, Sweden.
[45]V. Romero-Garcia, G. Theocharis, O. Richoux, and V. Pagneux, J. Acoust. Soc. Am. **139**, 3395 (2016).
[46]F. Wu, Y. Xiao, D. Yu, H. Zhao, Y. Wang, and J. Wen, Appl. Phys. Lett. **114**, 151901 (2019).
[47]M. Duan, C. Yu, Z. Xu, F. Xin, and T. J. Lu, Appl. Phys. Lett. **117**, 151904 (2020).

Published under license by AIP Publishing